Pergamon

Journal of Structural Geology, Vol. 16, No. 12, pp. 1675 to 1690, 1994

0191-8141/94 $7.00+0.00

0191-8141(94)E0040-6

Slip distributions on faults: effects of stress gradients, inelastic deformation, heterogeneous host-rock stiffness, and fault interaction

ROLAND BÜRGMANN and DAVID D. POLLARD

Department of Geological and Environmental Sciences, Stanford University, Stanford, CA 94305-2115, U.S.A.

and

STEPHEN J. MARTEL

Department of Geology and Geophysics, University of Hawaii, 2525 Correa Road, Honolulu, HI 96822, U.S.A.

(*Received* 13 *September* 1993; *accepted in revised form* 18 *January* 1994)

Abstract—Fault slip distributions are commonly assumed to be symmetrical about a central slip maximum, however, slip distributions in nature are often asymmetric. Although slip along an idealized fault is expected to follow an elliptical distribution after a single slip event in an elastic material, the slip distribution may be modified if the fault propagates or if additional slip events occur. Analytically and numerically computed fault-slip distributions in an elastic medium indicate that: (1) changes in the (frictional) strength along a fault; (2) spatial gradients in the stress field; (3) inelastic deformation near fault terminations; and (4) variations of the elastic modulus of the host rock can cause strong deviations from idealized symmetrical distributions along single-slip event faults. A relatively stiff body adjacent to or cut by a fault will tend to reduce fault slip in its vicinity and tends to flatten the slip profile where it is cut by the fault. Sharp slip gradients develop near the interface between relatively soft and stiff materials. The interaction of faults within about one fault radius of one another can strongly influence slip gradients. Inelastic processes, caused by stress perturbations in the stepover region of echelon faults, may link individual segments and thereby create a slip distribution resembling that of a single fault.

INTRODUCTION

FAULT slip distributions play an important role in earthquake studies, structural restorations of faulted terrain, and problems related to the flow of water or hydrocarbons in faulted reservoirs and aquifers. The distribution of slip along a fault depends on its geometry and that of neighboring structures, the remote boundary conditions and boundary conditions along the fault(s), and the constitutive behavior of the surrounding host rock. However, most studies of fault slip distributions neglect or greatly simplify the mechanical basis of this problem. Here we compute slip distributions for somewhat more realistic geometries, materials, and boundary conditions in order to define first-order factors that can influence fault slip.

Structural discontinuities, such as joints, dikes, solution surfaces, and faults, separate points (e.g. P and Q that initially were arbitrarily close to one another) by the difference of their individual displacement vectors ($\mathbf{u}[P]$, $\mathbf{u}[Q]$). This difference is defined as the *displacement discontinuity* (Fig. 1a):

$$\mathbf{D} = \mathbf{u}[P] - \mathbf{u}[Q].$$

The two planar surfaces that contain the displaced points are bounded in extent at a common *periphery* and can be idealized as a simple crack, for example in an elastic solid (Pollard & Segall 1987).

In two dimensions the components of the displacement discontinuity are:

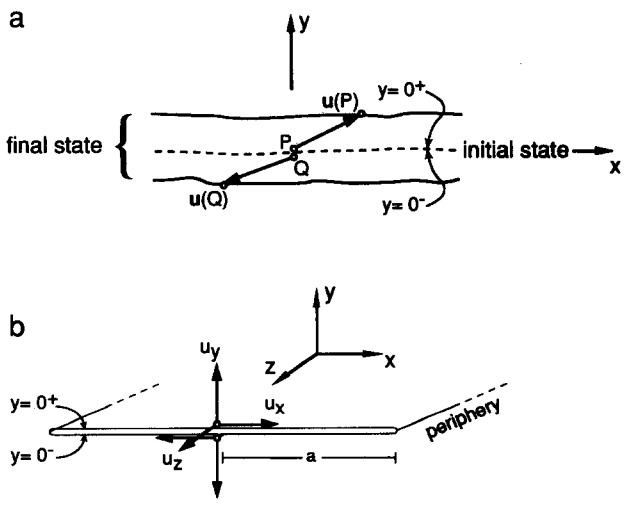

Fig. 1. Schematic illustration of a structural discontinuity. (a) The difference between displacement vectors of two originally neighboring points, $\mathbf{u}[P] - \mathbf{u}[Q]$, serves to define the vector displacement discontinuity, **D**. (b) Displacement components on faces of a two-dimensional crack of half-length as shown in the initial state.

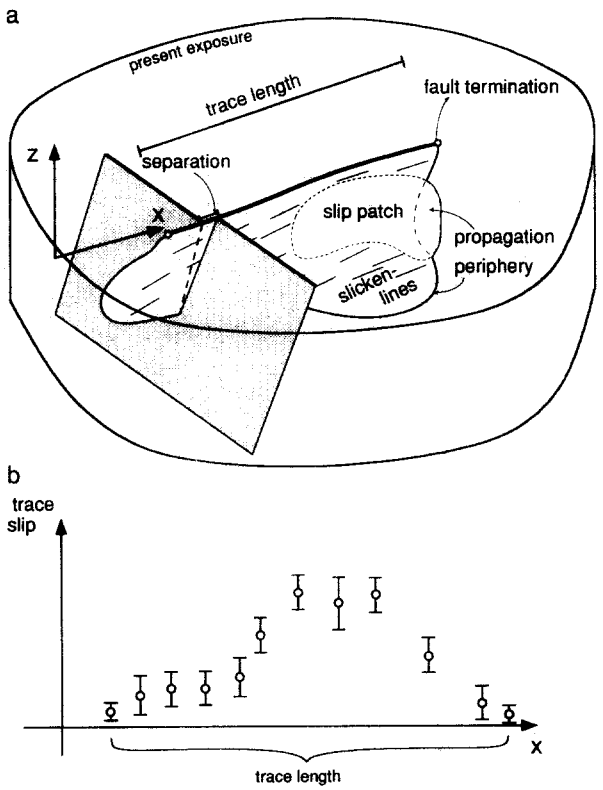

Fig. 2. (a) Schematic illustration of a three-dimensional fault with irregular periphery. The orientation of the slip vector is indicated by slickenlines or offset linear markers; the slip magnitude can be determined from offset linear or planar markers. (b) The quality of observed slip distributions along a fault trace depends strongly on the exposure, the number of markers, and the measurement method. Error bars indicate one standard deviation from mean value (circle).

$$D_x = u_x(|x| \le a, y = 0^+) - u_x(|x| \le a, y = 0^-),$$

$$D_y = u_y(|x| \le a, y = 0^+) - u_y(|x| \le a, y = 0^-).$$

If the displacement components parallel to the fracture surface of length $2a$ are much larger then the out-of-plane displacement components ($u_x \gg u_y$ and $u_z \gg u_y$), the resulting structural discontinuity is referred to as a *fault* and the in-plane displacement discontinuity is referred to as the *slip*.

Relative motions of the opposing surfaces of a fault commonly include a small fault-perpendicular component, manifest in fault gouge zone formation and dilation or compaction features (Aydin 1978, Antonellini *et al.* 1994). This relative motion may play an important role in fault development and propagation, but is ignored here.

Measurements of slip along the exposed trace of a fault usually provide limited information about the slip distribution over the three-dimensional fault surface (Fig. 2a). Only in a few cases, such as multiple exposures of faults on several mine levels (Rippon 1985) or the seismic imaging of many offset marker beds (e.g. Barnett *et al.* 1987, Bouvier *et al.* 1989, Chapman & Meneilly 1991, Walsh & Watterson 1991), can one determine the slip distribution over much of a fault plane. Linear geologic or cultural markers or planar offset markers used in conjunction with slip direction indicators on the fault plane (Petit 1987), constrain the magnitude and orientation of the displacement discontinuity vector (Fig. 2a).

Measurements of slip distributions depend on abundant displaced markers. When measuring slip gradients along recently active faults at the earth's surface, we rely on offset cultural features and geomorphic markers (Lawson 1908, Sieh 1978), and on displacements of geodetic bench marks (Thatcher & Lisowski 1987). Geophysicists can infer slip distributions in the subsurface from teleseismic and strong motion measurements and from geodetic data (e.g. Archuleta 1984, Harris & Segall 1987, Wald *et al.* 1990, Beroza 1991). The precision of slip measurements depend on the methods used, so the estimated precision should be shown with the measured values (Fig. 2b).

During a single slip event, slip may occur along only part of a fault surface. We refer to the portion of a fault that slips during one slip event as a slip patch (Fig. 2a). Some slip patches may enlarge the fault surface by *propagating* into the previously unfaulted host rock. The slip distribution during a single event is related to various factors, including the slip-patch dimensions and shape of its periphery, stress perturbations due to previous slip events, material properties of the host rock and fault zone, geometric irregularities along the fault, and the orientation of the measured transect relative to the fault service. These factors also influence the slip rates on creeping, or actively slipping faults (e.g. Li 1987, Bilham & Bodin 1992). For example, Bilham and King (1989b) used numerical models to show that earthquake slip is commonly reduced along oblique fault segments.

Repeated ruptures of various slip patches produce the total slip distribution on a multi-event fault. This final slip distribution is affected not only by the parameters influencing slip during a single slip event, but also by additional factors, including temporal material and stress-field changes, the development of permanent strain in the host material, and the effects of fault growth (Muraoka & Kamata 1983, Rippon 1985, Higgs & Williams 1987, Walsh & Watterson 1987, 1988, 1989, Cowie & Scholz 1992a).

Most studies to date of slip distributions and the relationship between fault length and fault slip magnitude assume simple models with isolated faults and homogeneous material properties and loading. For these models the maximum slip is in the middle of the fault, and decreases, according to a smooth function, to zero at the fault ends (e.g. Walsh & Watterson 1988, Cowie & Scholz 1992b). While some observed slip distributions can be roughly approximated by such models (Rippon 1985, Barnett *et al.* 1987, Dawers *et al.* 1993) there are many asymmetric and complex examples that suggest further analysis (Rippon 1985, Peacock 1991, Walsh & Watterson 1990, 1991, Dawers *et al.* 1993).

Somewhat more complex models were developed by Pollard and Muller (1976) who used analytical solutions for an opening crack subject to linear stress gradients to explain the teardrop shape of some igneous dikes and

sills. They pointed out that the commonly observed asymmetrical shapes of sheet intrusions may be related to: (1) regional stress gradients; (2) magma pressure gradients; (3) changes in host rock stiffness along the intrusions; and (4) the irregular three-dimensional geometry of intrusions. Delaney & Pollard (1981) used a numerical model to analyze the opening of echelon dike segments and showed how mechanical interaction among the segments could explain their shape. In this contribution we use analogous concepts for shearing cracks to analyze slip distributions along faults.

Our results are based on analytical solutions using published stress functions (Tada *et al.* 1973) and numerical boundary element models (Crouch & Starfield 1983). In particular we consider gradients of stress along a fault (due to variable friction or a spatially varying remote stress field) and inelastic secondary structures that may form due to stress perturbations at fault ends. We focus on the interaction of fault segments in an echelon arrangement and the effects of inelastic deformation at stepovers. We also examine how slip distributions can be affected by heterogeneity in the elastic modulus of a rock mass cut by a fault. Our goal is to show how these factors, in addition to probable effects of irregular three-dimensional fault shapes, can play a significant role in determining the slip distribution along faults.

MEASURED SLIP DISTRIBUTIONS AND ELEMENTARY MODELS

Single-slip-event fault displacements

Measured slip distributions of single-slip earthquake events typically are complex (Fig. 3). These distributions commonly show multiple maxima, asymmetric slip distributions, changes in slip vector orientation, and irregular gradients (e.g. Lawson 1908, Sieh 1978, Archuleta 1984, Rymer 1989, Wald *et al.* 1990, Beroza 1991). Some complexity in slip distributions can be correlated to fault geometry, in which individual fault segments are often arranged in an echelon fashion, with associated conjugate faults and fault steps and bends at all scales (Tschalenko 1970, Vedder & Wallace 1970, Wallace 1973, Bilham & King 1989a,b, Bilham & Bodin 1992). For example, the slip distribution determined for the 1987 Superstition Hills earthquake sequence (Rymer 1989, Wald *et al.* 1990) shows the effects of stress field perturbations from a previous rupture and the interaction of two echelon fault segments (Fig. 3).

One of the most elementary models of a single slip event on a fault predicts an elliptical slip distribution in a linear elastic, homogeneous, isotropic, and isothermal material (Pollard & Segall 1987). This two-dimensional model assumes that the regional stress field is uniform, that shear tractions on the fault surfaces are constant, and that no fault propagation occurs.

The displacement discontinuity (slip) along such a model fault (Fig. 4a inset) may be derived utilizing Westergaard's (1939) simplification of Muskhelishvili's

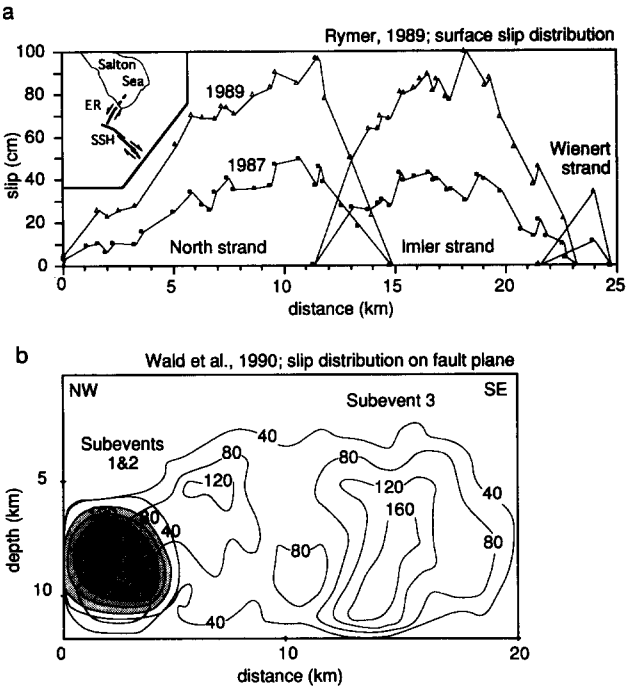

Fig. 3. (a) Slip distribution from single-slip events measured along the 1987 Superstition Hills earthquake rupture (SSH) at the earth's surface immediately following (squares) and two years after (triangles) the earthquake (after Rymer 1989). Aseismic shallow afterslip approximately doubled the original surficial offsets to roughly match the magnitude of slip at depth. (ER—Elmore Ranch fault.) (b) The slip distribution of the 1987 Superstition Hills earthquake determined from seismologic strong motion data (after Wald *et al.* 1990), slip contours are in centimeters. Three slip events can be distinguished. Only the third broke the whole length of the fault, about 8 *s* after the first event that may have ruptured in response to a previous event on the left-lateral Elmore Ranch fault, oriented perpendicular to the Superstition Hills fault which occurred about 11 h earlier (Fig. 3a inset). The final rupture of the two major fault segments initiated at the NW-fault termination and resulted in a slip distribution with two distinctive peaks.

general solution for an elliptical cavity in an infinite elastic body (Muskhelishvili 1954, pp. 347–358). The method uses functions of a complex variable ($z = x + iy$) to find an analytical stress function $Z(z)$ that satisfies the equilibrium and compatibility equations and stress–strain relations for a linear elastic material, as well as the boundary conditions of a given problem. Using the appropriate Westergaard stress function one can calculate the stress and displacement fields in the body surrounding a crack (Tada *et al.* 1973). For example, the two-dimensional, plane strain displacement components in the (x, y)-plane for any loading that produces a displacement discontinuity in the u_x-component across the crack are:

$$u_x = \frac{1}{2G}[2(1-\nu)\,\mathrm{Im}\,\bar{Z} + \mathrm{Re}\,Z] \qquad (1a)$$

$$u_y = \frac{1}{2G}[-(1-2\nu)\,\mathrm{Re}\,\bar{Z} - y\,\mathrm{Im}\,Z], \qquad (1b)$$

where the model fault occupies a straight segment on the x-axis from $x = -a$ to $x = +a$ (Fig. 4a inset), G is the shear modulus, ν is Poisson's ratio, $Z = (d/dz)\bar{Z}$, and Im and Re refer to the imaginary and real parts of these

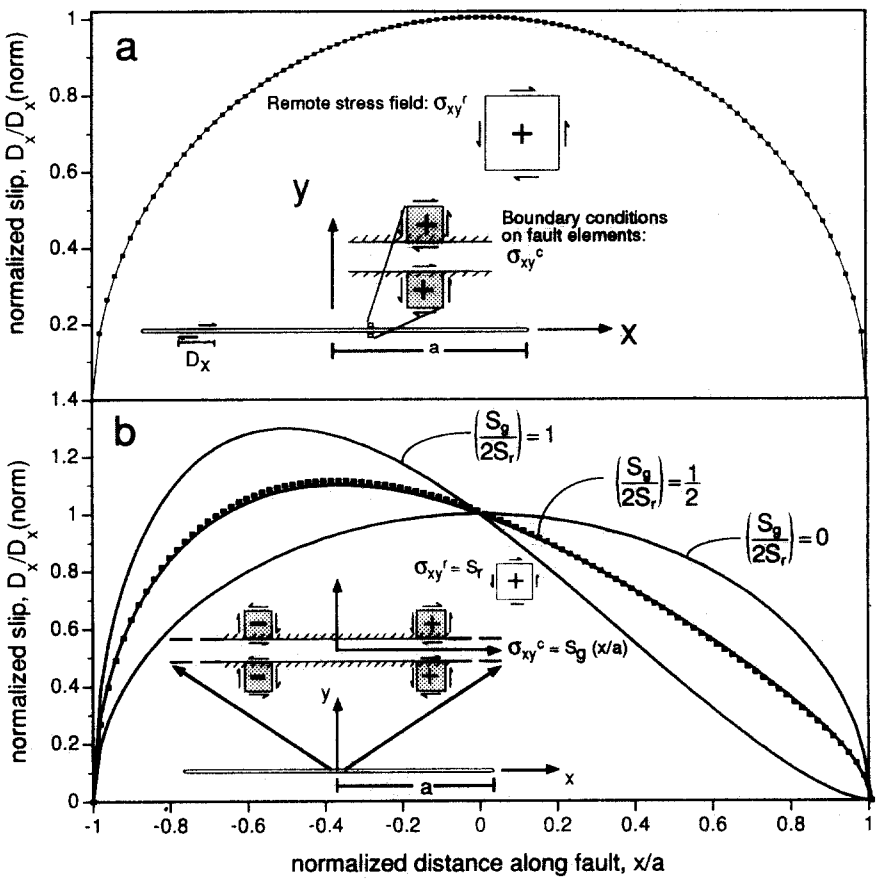

Fig. 4. (a) The analytically (solid curve) and numerically (squares) computed displacement discontinuity **D** along an isolated fault in an infinite body after a unit shear-stress drop. The boundary element numerical model consists of 100 uniform slip elements with prescribed stress boundary condition. Inset shows boundary conditions and geometry for a crack, the model fault surface, in an elastic, isotropic, and homogeneous material. The coordinates are aligned with the crack and the origin is at the crack center. Distance, x, along the fault trace is normalized by fault half-length, a. (b) Effects of a linear stress distribution along a model fault. Plot of normalized slip vs normalized distance using equation (8). The parameter $S_g/2S_r$ controls the relative magnitudes of the linear and uniform stresses loading the model fault. For comparison we plot the numerical (small squares) solution for $S_g/2S_r = 0.5$. Boundary conditions are shown in the inset.

functions, respectively (Tada *et al.* 1973, p. 1.23). Such a case corresponds to the mode-II classification of fracture mechanics (Lawn & Wilshaw 1975, p. 52) where the relative motion is in the crack plane and perpendicular to the crack periphery.

In the case of an applied uniform remote shear stress σ^r_{xy} and no tractions on the crack faces the stress function is:

$$Z(z) = \frac{\sigma^r_{xy}}{\sqrt{z^2 - a^2}}, \qquad (2)$$

where a is the crack half length (Westergaard 1939). The displacement component on the upper crack face ($|x| \leq a$, $y = 0^+$) is found from equation (1a) to be

$$u_x = \frac{(1-\nu)}{G} \operatorname{Im} \bar{Z}. \qquad (3)$$

Substituting equation (2) into equation (3) we find:

$$u_x(|x| \leq a, y = 0^+) = \sigma^r_{yx} \cdot \frac{(1-\nu)}{G} \cdot \sqrt{a^2 - x^2}. \qquad (4)$$

On the opposite crack face u_x is equal in magnitude but opposite in sign, thus producing a displacement discontinuity, **D** given by twice the value of u_x in equation (4). A positive σ^r_{yx} produces right-lateral slip on the model fault.

For a uniform shear traction acting on the crack face in the x-direction and no stress in the remote field, the displacement component, u_x, on the crack face is of the same form as equation (4). However, if this shear traction induces a positive shear stress, σ^c_{yx}, the model fault slips in a left-lateral sense (Fig. 4a, inset). Thus the displacement discontinuity (slip) along a single fault of length $2a$ with a uniform traction on the faces of magnitude σ^c_{yx} and a uniform remote stress σ^r_{yx} is

$$D_x = 2(\sigma^r_{yx} - \sigma^c_{yx}) \cdot \frac{(1-\nu)}{G} \cdot \sqrt{a^2 - x^2}, \qquad (5)$$

where $(\sigma^r_{yx} - \sigma^c_{yx})$ is the constant shear-stress drop along the model fault (Fig. 4a). A positive D_x refers to a right-lateral sense of slip. The displacement discontinuity in the y-orientation (mode-I opening or interpenetration of the crack walls) and in the z-orientation (mode-III sliding) are zero.

From equation (5) the slip magnitude follows an elliptical distribution and is linearly proportional to the length of the fault and to the shear-stress drop. The slip is inversely proportional to the elastic shear modulus.

The maximum displacement discontinuity occurs at the center of the model fault and goes to zero at the ends (Fig. 4a). Following the result in equation (5), we normalize all the plotted slip distributions for our models by the maximum for this base case, where

$$D_x(x = 0;\ \sigma^c_{yx} = 0) = D_x(\text{norm}) = 2(\sigma^r_{yx})\frac{(1-\nu)}{G}a.$$

In the case of a three-dimensional fault the slip distribution has an elliptical form if the fault has an elliptical periphery and one of the axes is parallel to the direction of shear-stress drop (Eshelby 1957);

$$D_x = \frac{8b}{\pi}(\sigma^r_{yx} - \sigma^c_{yx}) \cdot \left(\frac{(1-\nu)}{G(2-\nu)}\right) \cdot \sqrt{1 - \frac{x^2}{a^2} - \frac{z^2}{b^2}}. \quad (6)$$

The displacement discontinuity in the z-direction, D_z is zero [here z refers to the other co-ordinate in the crack plane (Fig. 2a), and has no relation to the complex z]. Faults of a more complex shape, or elliptical faults whose axes are oriented oblique to the shear stress drop, will have more complex slip distributions. The simple two- and three-dimensional models provide a standard against which more complex cases can be judged. We will restrict our attention to two-dimensional plane-strain examples.

Fault slip results in stress concentrations around the fault termination. The stress intensity factors K_{I}, K_{II}, and K_{III} represent the strength of the stress field surrounding a crack tip in opening, in-plane shearing, and tearing displacement discontinuity modes, respectively (Lawn & Wilshaw 1975, p. 51). The stress intensity factors are proportional to the applied stresses and are determined by the stress boundary conditions and the geometry of a given problem. Only if all three stress intensity factors are zero do we not find a stress singularity at a crack tip. If any stress intensity factors are not zero, the stress concentration may cause the material to fail inelastically and allow the crack to propagate. The stress intensity factor for the elementary two-dimensional fault model is

$$K_{\text{II}} = \sigma^r_{yx}\sqrt{\pi a}. \quad (7)$$

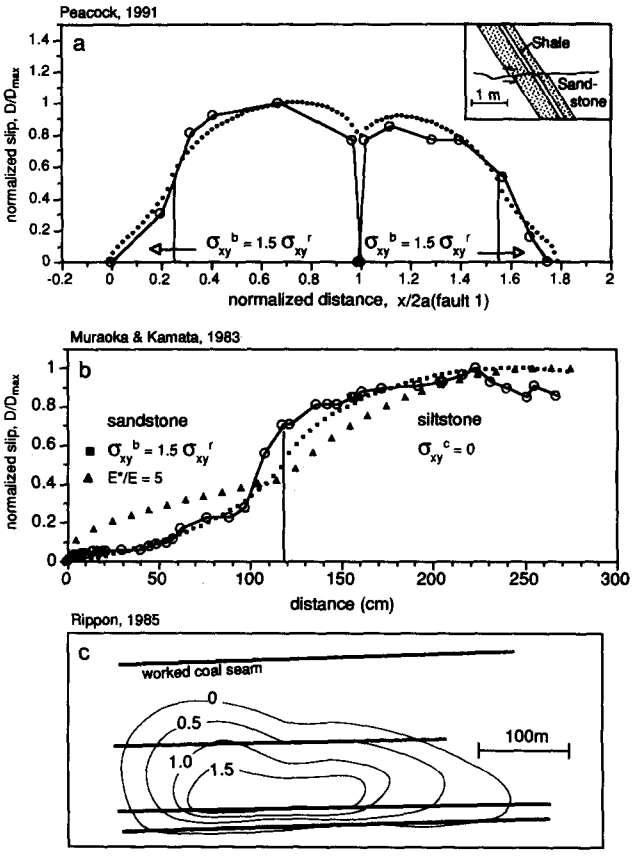

Fig. 5. Cumulative slip distributions measured along faults exposed in mines or along outcrops that provide abundant offset markers. (a) Normalized slip (open circles, D_{max} = 65 mm) along two right stepping left-lateral strike-slip faults (inset) near Kirkcudbright, Scotland (after Peacock 1991). Note the high slip gradient where the two fault segments interact. The step is contained in a shale bed. Shown for comparison is a model of fault interaction and inelastic deformation near fault discontinuities. Inelastic deformation in the fault step, and frictional end zones near the distal fault ends provide a good model fit. (b) Normalized slip distribution along a normal fault (open circles, D_{max} = 86 mm) cutting across layered Quaternary sediments near Kyushu, Japan (after Muraoka & Kamata 1983). The slip along the normal fault drops sharply proceeding down dip from the siltstone to the sandstone. Shown for comparison are a model where the sandstone has a Young's modulus five times of that of the host rock (triangles) and a model of increased frictional resistance of the fault segment in the sandstone bed (squares). (c) Contoured three-dimensional distribution of vertical displacements derived from measured offsets of coal and sandstone beds on several levels of a mine in northeast Derbyshire (after Rippon 1985). The normal fault steepens from about 40° at its center to 60° near its lower termination. The down-dip slip distribution along this fault may be influenced by down-dip and lateral steepening, effects of changing host rock properties, and fault segmentation.

Cumulative fault displacements

Measured cumulative slip distributions along faults often are distinctly non-elliptical and consequently a number of researchers have developed fault models to explain and categorize such distributions (Muraoka & Kamata 1983, Higgs & Williams 1987, Walsh & Watterson 1987, 1988, 1989, Peacock 1991, Cowie & Scholz 1992a). Non-elliptical slip distributions have been attributed to the effects of fault growth and appear to be affected by lithologic variations (Figs. 5a & b), fault interaction (Fig. 5a), and bends along the fault trace (Fig. 5c) (Muraoka & Kamata 1983, Rippon 1985, Peacock 1991, Walsh & Watterson 1990, 1991, Cowie & Scholz 1992a).

One class of modifications to the elementary elastic models (Fig. 4a), motivated by non-elliptical slip distributions, involves the introduction of fault propagation with each slip event (Watterson 1986, Walsh & Watterson 1987, Cowie & Scholz 1992a). Modeled slip in a single event increases linearly with fault length (equation 5). If the whole growing fault slips during each event, the cumulative slip distribution can be considered to be made up of the sum of individual, elliptical, distributions at each growth stage (Watterson 1986). This implies that stress perturbations resulting from slip relax by permanent straining between each slip event. The form of the resultant slip distribution depends on

the size of the fault growth increments (Watterson 1986, Walsh & Watterson 1987, Cowie & Scholz 1992a,b, Gillespie *et al.* 1992) and is symmetric.

SLIP DISTRIBUTIONS ON SINGLE FAULTS WITH NON-UNIFORM STRESS DROPS

One mechanism which may cause deviations from the simple model of slip distribution is related to non-uniform stress drop along faults. This may be the result of a non-uniform remote stress field or the result of varying frictional resistance or cohesion. Here we use analytical slip distributions from linear stress-drop distributions along faults, distributions modified by the effects of increased frictional resistance near fault terminations, and distributions caused by a linear increase of frictional resistance from the fault center.

Linear stress distributions along single faults

We analyze the influence of non-uniform loading on slip distributions by imposing spatially varying stress boundary conditions in the remote field or along a fault. Spatially variable stress fields on all scales are likely the norm, rather than the exception, in actively deforming tectonic settings (e.g. Zoback & Zoback 1991, Reasenberg & Simpson 1992). First we analyze the effects of a linear stress distribution along a fault. This may approximate conditions where a fault has propagated through materials of varying coefficient of friction. In the remote field $\sigma^{r}_{yx}\ (x,\ y \to \infty) = \text{const.} = S_r$ and on the fault surfaces the traction varies linearly such that the stress is $\sigma^{c}_{yx}\ (|x| < a,\ y = 0\pm) = S_g\ (x/a)$.

The slip distribution is:

$$D_x = \frac{(1-\nu)}{G}\left[2S_r - S_g\left(\frac{x}{a}\right)\right] \cdot \sqrt{a^2 - x^2}. \qquad (8)$$

A linear distribution of the shear traction on the fault provides resistance to slip along one side ($x > 0$) and enhances slip on the other side ($x < 0$) relative to the base case of a uniform stress drop. This results in a skewed or tear-drop slip distribution with the maximum slip centered off the middle of the fault (Fig. 4b). As the ratio $S_g/2S_r$ increases from 0 to 1 the asymmetry in slip becomes more pronounced. In the limiting case for right-lateral slip where $S_g/2S_r = 1$ the slip asymptotically approaches zero at $x = +a$. For greater values of the ratio, the right-hand side of the model fault slips in a left-lateral (negative) sense. It is worth noting that the mode II stress intensity is

$$K_{II} = (S_r \pm \tfrac{1}{2}S_g)\sqrt{\pi a},\ x = \pm a.$$

The stress singularity at ($x = +a$) disappears ($K_{II} = 0$) in the limiting case where $S_g/2S_r = 1$. We will return to this phenomenon after introducing the end zone models.

Non-linear stress distributions: an end zone model

Non-uniform or non-linearly varying remote shear stress distributions or changes in frictional strength along faults may occur in particular tectonic settings or may be caused by particular mechanisms for fault propagation and frictional resistance to slip. It has been suggested that, as a fault propagates through previously intact soil or rock, a particular section of the fault will develop from an immature zone of relatively great strength (or friction) at the fault termination to a well-developed fault zone of lower strength (Ida 1972, Palmer & Rice 1973, Rudnicki 1980, Li 1987). More recently, Cowie & Scholz (1992b) have adopted these concepts in discussions of slip distributions on faults.

The increased resistance to slip may be related to inelastic deformation in a volume of rock surrounding the fault termination (Cowie & Scholz 1992b) or to greater friction between fault surfaces because of microstructural processes (Palmer & Rice 1973) and geometrical irregularities of the fault surfaces. In any case, the increased resistance at fault terminations leads to slip distributions that show more tapering near the fault terminations than predicted for a uniform stress drop (Fig. 4a).

We consider a simple end-zone fault model with uniform remote shear stress, σ^{r}_{yx}, uniform shear stress, σ^{m}_{yx}, over the central portion of the fault, and end zones with uniform shear stress, σ^{c}_{yx}, (Fig. 6a, inset). Cowie & Scholz (1992b) studied a similar distribution of normal stresses using the Barenblatt (1962) opening-mode equations as an analogue for faults. We compute the effects of the non-uniform loading on fault patches using Westergaard stress functions from Tada *et al.* (1973, p. 5.11). Because the linear–elastic stress fields and the related stress functions are additive, solutions for the different loading configurations are superimposed. The displacement discontinuities for the three different applied shear stresses are:

Case 1. Stress-free crack of length $2a$ under remote uniform loading, $\sigma^{r}_{yx} = S_r$:

$$D_x = 2S_r \cdot \frac{(1-\nu)}{G}\sqrt{a^2 - x^2}. \qquad (9)$$

Case 2. Uniform stress of magnitude $\sigma^{m}_{yx} = S_m$ along the central portion of the fault ($-d \le x \le +d$, Fig. 6a inset);

$$D_x = -\frac{2(1-\nu)}{\pi G} S_m \times \left[\begin{array}{l} (d-x)\cosh^{-1}\left\{\dfrac{a^2 - dx}{a|x-d|}\right\} \\ + (d+x)\cosh^{-1}\left\{\dfrac{a^2 + dx}{a|x+d|}\right\} \\ + 2\sin^{-1}\left(\dfrac{d}{a}\right)\sqrt{a^2 - x^2} \end{array}\right]. \qquad (10)$$

Case 3. Uniform stress of magnitude $\sigma_{yx}^{c} = S_c$ along two end zones ($d < |x| \leq a$) at either end;

$$D_x = -\frac{2(1-\nu)}{\pi G} S_c \times \left[\begin{array}{l} (d+x)\cosh^{-1}\left\{\dfrac{a^2 - dx}{a|x-d|}\right\} \\ + (d-x)\cosh^{-1}\left\{\dfrac{a^2 + dx}{a|x+d|}\right\} \\ + 2\left\{\dfrac{\pi}{2} - \sin^{-1}\left(\dfrac{d}{a}\right)\right\}\sqrt{a^2 - x^2} \end{array} \right]. \quad (11)$$

Adding the three terms we find

$$D_x = \frac{2(1-\nu)}{G} \times \left[\begin{array}{l} \left\{(S_r - S_c) - (S_m - S_c)\dfrac{2}{\pi}\sin^{-1}\left(\dfrac{d}{a}\right)\right\}\sqrt{a^2 - x^2} \\ -\dfrac{1}{\pi}(S_m - S_c)\left\{ \begin{array}{l} (d+x)\cosh^{-1}\left(\dfrac{a^2 + dx}{a|x+d|}\right) \\ + (d-x)\cosh^{-1}\left(\dfrac{a^2 - dx}{a|x-d|}\right) \end{array} \right\} \end{array} \right]. \quad (12)$$

This rather complex distribution reduces to the expected end-members. For example, as $d \rightarrow a$, D_x reduces to equation (5) with a uniform stress drop of $(S_r - S_m)$, and as $d \rightarrow 0$, D_x reduces to equation (5) with a uniform stress drop of $(S_r - S_c)$. In general, the slip distribution depends on the three stress magnitudes and on the length of the end zone (Figs. 6a & b).

Of particular interest are cases where the stress concentration near the fault termination is finite; that is, the stress intensity factor $K_{II} = 0$ (Rudnicki 1980). Adding the stress intensity factors given by Tada *et al.* (1973) for the three cases described above, we find that $K_{II} = 0$ if

$$\frac{S_r - S_c}{S_m - S_c} = \frac{2}{\pi}\sin^{-1}\left(\frac{d}{a}\right). \quad (13)$$

This provides the relation among the three shear stresses and the geometric parameters of the fault for a fault growth criterion $K_{II} > 0$. For example, assuming $S_m/S_r = 0$ and $S_c/S_r = 1.5$, the geometry $d/a = 0.5$ corresponds to a zero slope in the slip distribution at the terminations and yields the condition $K_{II} = 0$.

A special case stems from the work on *cohesive* end zones near the terminations of opening-mode cracks by Barenblatt (1962) and on plastic end zones for opening cracks by Dugdale (1960). By analogy to their results, certain distributions of shear stress in the cohesive zone of a shearing-mode crack will oppose the action of the remotely applied load so as to eliminate the stress singularity at the model fault termination. For these cases the stress intensity factor K_{II} is zero (Rudnicki 1980). The criterion originally proposed by Barenblatt (1962) for opening-mode cracks specifies K_I is zero.

If a volume of rock surrounding the fault termination experiences inelastic deformation and it is small compared to the volume in which the stress would be approximated by the so-called near-tip field, the principles of linear elastic fracture mechanics (LEFM) apply (Kanninen & Popelar 1985, p. 146). The near-tip field is a good approximation for the elastic stress within a radius r of a fracture tip if $r < 0.01$ a (Pollard & Segall 1987, p. 342). Under these limiting conditions of *small scale yielding* it is meaningful to consider a propagation criterion based on the stress intensity factor and to calculate slip distributions using a purely elastic solution. The tapered portion of the slip distribution would be confined to very near the terminations of the fault. On the other hand, if the greater resistance to slip is provided by friction on the fault, there is no limit to the size of the surface so affected and the tapering could extend to the fault center.

Li (1987, pp. 383–389), Rudnicki (1980, p. 498), and Martel & Pollard (1989) discuss some theoretical and experimental constraints on the length of the end zone, but there are few good constraints on what the length of an end zone for a natural fault might be, or what an appropriate stress distribution along a developing fault might be. Cowie & Scholz (1992a) propose a model wherein the normalized length of the end zone $(a-d)/a$ is constant as a fault grows. This implies that a critical displacement is required to weaken the breakdown zone which scales with the dimension of the fault.

A symmetric linear stress distribution

Increased strength or friction along a fault may be limited to a small zone near the fault terminations or may decrease more gradually towards the region of greater displacement near the fault center. To remain in the context of our models this shear strength must not be exceeded except within the fault itself so the surrounding material is elastic. We examine the possible effects of gradual changes in the resistance to slip towards the fault ends using the Westergaard function for a symmetric linear stress distribution (Tada *et al.* 1973, p. 5.14). In the remote field $\sigma_{yx}^{r}(x, y \rightarrow \infty) = \text{const.} = S_r$, and $\sigma_{yx}^{c}(|x| \leq a,\ y = 0^{\pm}) = S_g(|x|/a)$ on the fault surfaces. The displacement discontinuity is given by:

$$D_x = \frac{(1-\nu)}{G} 2\left[S_r\sqrt{a^2 - x^2} - S_g\frac{1}{\pi}\left\{\sqrt{a^2 - x^2} + \frac{x^2}{a}\cosh^{-1}\left(\frac{a}{x}\right)\right\}\right]. \quad (14)$$

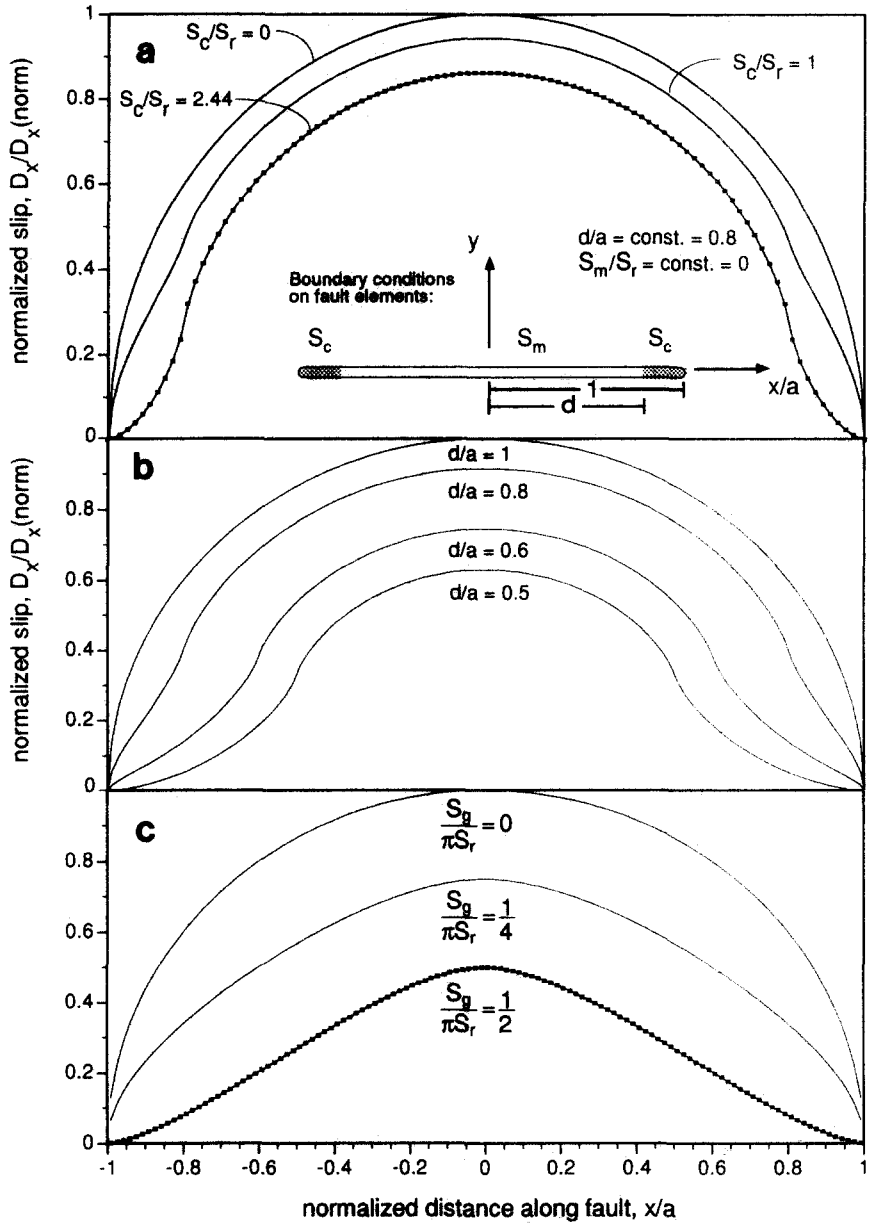

Fig. 6. Effects of non-linear stress distributions along a model fault with a weak center portion and stronger end zones. (a) Normalized slip distributions with $d/a = 0.8$ and $S_m/S_r = 0$ for a range of end-zone stresses $0 \leq S_c/S_r \leq 2.44$. The zero slope of the displacement curve at the fault termination for $S_c/S_r = 2.44$ corresponds to the $K_{II} = 0$ condition given in equation (13). The numerical model for $S_c/S_r = 2.44$ (squares) closely reproduces the analytical result. The boundary conditions and geometry are shown in the inset. (b) Normalized slip distributions with $S_m/S_r = 0$ and $S_c/S_r = 1.5$ for end zone lengths, $0.5 \leq d/a \leq 1$. (c) Effects of linear symmetric stress distributions along a model fault. Normalized slip distributions for a range of stress gradients $0 \leq S_g/\pi S_r \leq 0.5$. The numerical model for $S_g/\pi S_r = 0.5$ (squares) closely reproduces the analytical result. If $S_g/\pi S_r > 0.5$, slip will be left-lateral near the fault terminations; if $S_g/\pi S_r < 0$ slip is enhanced towards the fault ends.

The mode II stress intensity factor is:

$$K_{II} = \left(S_r - S_g \frac{2}{\pi}\right)\sqrt{\pi a}. \tag{15}$$

So the condition of Barenblatt, $K_{II} = 0$, is obtained at both terminations when

$$\frac{S_g}{\pi S_r} = \frac{1}{2}. \tag{16}$$

If $\sigma_{yx}\ (x = \pm a,\ y = 0^+) = S_g$ is a measure of the shear strength of the fault near its termination, then the fault will propagate when $S_r \geq (2/\pi)S_g$ maintaining $K_{II} = 0$. The resulting modified slip distribution is shown as one of the curves in Fig. 6(c). This slip distribution shows a reduction of the maximum slip magnitude (~50% of the complete stress-drop model, $S_g = 0$) and a more linear (tapered) decrease towards the fault terminations, ending in a zero slope. Model faults such as those shown in Fig. 6 may explain the tapered form of slip observed along some natural faults (e.g. Walsh & Watterson 1987, 1989).

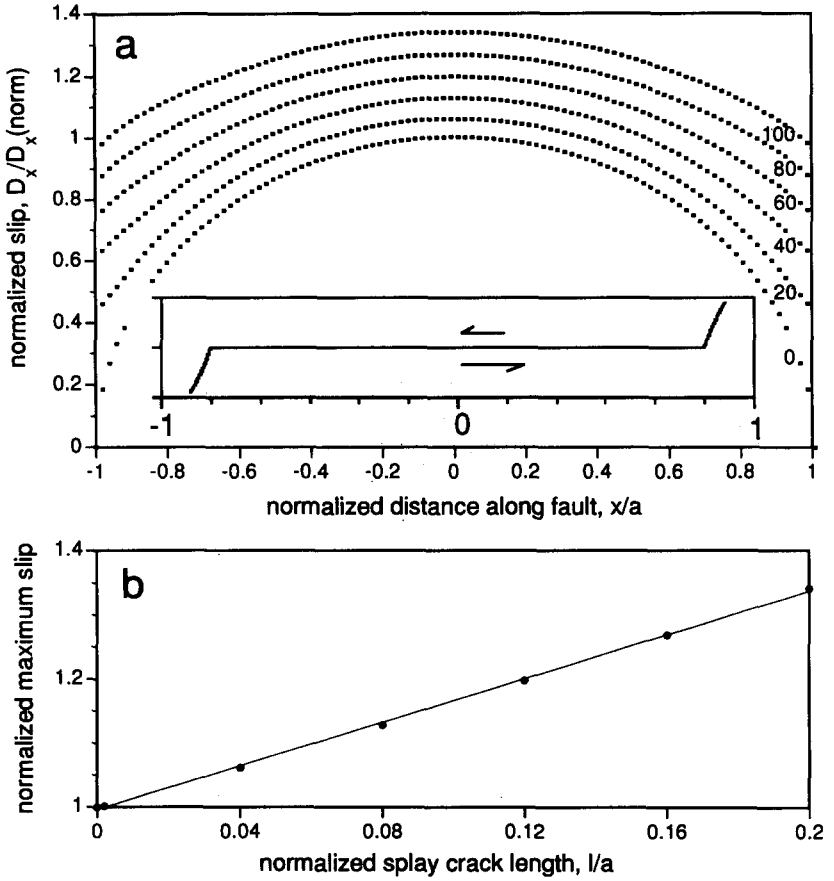

Fig. 7. Influence of inelastic deformation (opening splay fractures) at fault terminations on slip. A zero shear stress is specified as the boundary condition along the whole length of the fault resulting in a uniform 1 MPa stress drop. The newly formed elements are specified to carry zero shear- and normal tractions and their orientation is determined by the maximum circumferential stress criterion (Erdogan & Sih 1963, Thomas & Pollard 1993). The splay cracks initiate at an angle of approximately 70° to the x-axis and propagate at slowly decreasing angles away from the fault. (a) Slip distribution along faults with splay fractures at various stages of splay fracture growth (0, 20, 40, 60, 80 and 100 increments of 0.002a). The inset shows the fracture path through 100 growth increments. (b) Maximum slip magnitude at the center of the fault is approximately linearly related to the length of the splay fractures.

EFFECTS OF INELASTIC STRAIN AT FAULT ENDS, FAULT INTERACTION, AND HOST ROCK HETEROGENEITY ON SLIP DISTRIBUTIONS

We utilize the boundary element method (Crouch & Starfield 1983) to study the displacement distributions on faults under boundary conditions that are more complex than those described in the previous section. The program Frac2D (Thomas & Pollard 1993) allows us to study the plane, elastostatic stress and displacement fields about any number of fractures with varying loads and geometries. By imposing varying stress boundary conditions along the faults we can analyze the effects of variations in strength (friction or cohesion) along a fault. The addition of a second fault allows us to study the effects of mechanical interaction on slip distributions.

We test the accuracy of the numerical solution method through a comparison with the analytical results in Figs. 4 and 6. In each figure, the unbroken line represents the analytical solution, whereas the individual points are the numerical results computed for similar boundary conditions. Slip distributions in the numerical models very closely follow the analytical results.

Effects of inelastic deformation at fault ends

Commonly, stress concentrations at fault terminations favor the development of secondary structures: opening cracks, veins and normal faults in the extensional quadrant (Erdogan & Sih 1963, Nemat-Nasser & Horii 1982, Segall & Pollard 1983, Granier 1985, Deng *et al.* 1986, Petit & Barquins 1988, Martel *et al.* 1988, Barquins & Petit 1992), and pressure solution seams, thrust faults, folds, and ductile fabrics in the contractional quadrant (Fletcher & Pollard 1981, Deng *et al.* 1986, Bürgmann & Pollard 1992).

Opening-mode fracture growth is introduced with a fracture criterion at the model fault terminations (e.g. Lawn & Wilshaw 1975). These cracks are prescribed to grow by a small increment (0.002 a) if the mode I stress intensity factor, K_I, exceeds the critical stress intensity factor K_{Ic} = 1.5 MPa $m^{1/2}$ (Atkinson & Meredith 1987, p. 492).

With increasing splay-crack length, slip magnitude on the fault increases and the slip gradient near the fault terminations decreases (Fig. 7a). The slip magnitude on boundary elements near the fault termination is approximately equal to the opening displacement on the bound-

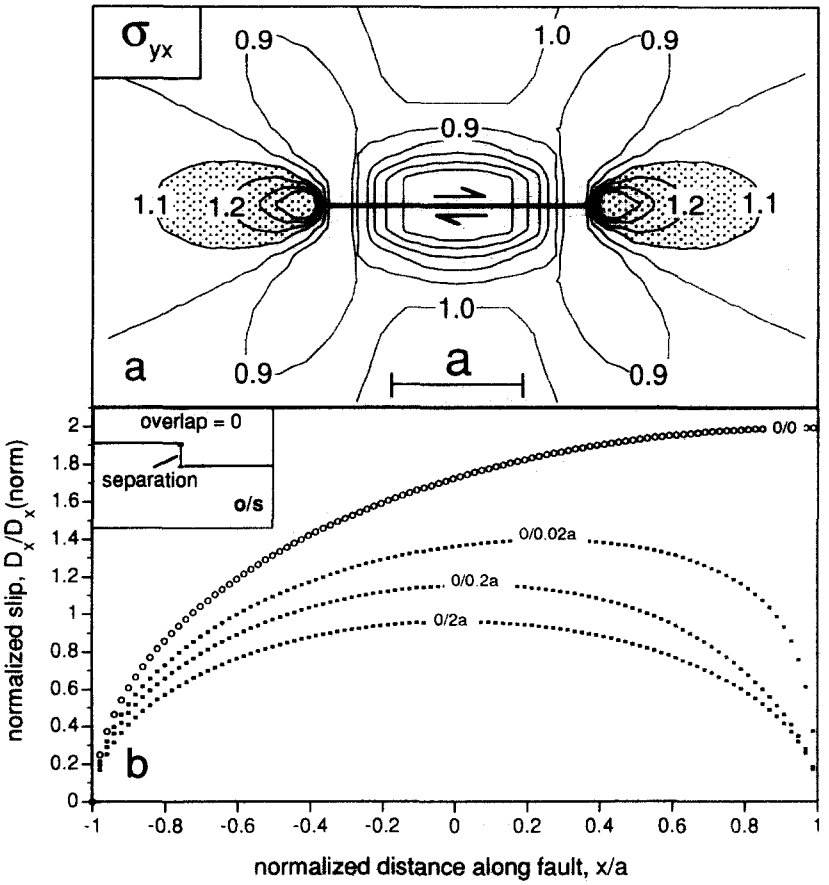

Fig. 8. (a) Contoured distribution of the fault-parallel shear stress, σ_{yx}, about a slipped fault. (b) Slip distribution along the left-most echelon segment of a pair of faults with zero overlap and various amounts of separation (0–2 times the fault half-length a). Each fault is discretized into 100 elements with zero-shear-stress and zero-normal-stress boundary conditions under a remote shear stress of 1 MPa. Fault slip is locally enhanced or diminished due to the effects of the local stress field.

ary elements near the base of the splay crack. The maximum slip magnitude near the center of the fault increases approximately linearly with splay crack length (Fig. 7b).

This analysis illustrates how inelastic deformation near fault terminations, due to opening fractures increase the slip magnitude along a fault and decrease the gradient in slip elsewhere along the fault. Furthermore, slip is not constrained to zero at the fault termination, if it is coupled to the inelastic deformation such as splay crack opening. If such inelastic deformation were to occur near one fault termination only, a highly asymmetric slip distribution would result.

Fault interaction across echelon steps

Faults are typically composed of individual fault segments in a left- or right-stepping echelon geometry (Wallace 1973, Crowell 1974, Segall & Pollard 1980, Christie-Blick & Biddle 1985, Aydin & Schultz 1990). The interaction of individual fault segments in an echelon arrangement leads to characteristic stress fields and resulting deformation patterns, depending on the left- or right-stepping character of fault stepovers for a given sense of shear (Rodgers 1980, Segall & Pollard 1980, Bilham & King 1989a, Aydin & Schultz 1990, Bürgmann & Pollard 1992). Here we analyze the effects of fault interaction across simple echelon fault steps on the slip distribution.

We model the slip distribution along two stress-free, frictionless faults; that is, fault strength is not dependent on the fault-normal stress. We illustrate the effects of fault interaction by calculating the slip distribution along two straight parallel faults of varying overlap and separation.

The fault segments interact by modifying the local stress field. Where the stress perturbation from slip on one fault (Fig. 8a) increases or decreases the shear stress, σ_{yx}, on its neighbor, the tendency will be to enhance or reduce slip in that region. The slip distributions will be the same for left- and right-stepping geometries due to the symmetric nature of the shear stress field.

The interaction of the echelon fault segments can cause asymmetric slip distributions along the faults, and the maximum slip magnitude may increase or decrease compared to that for the single fault model. The slip distribution depends on the amount of overlap of the two fault segments and their separation. With zero overlap, the slip magnitude on the individual faults decreases with increasing separation and the locus of maximum slip shifts toward the segment centers (Fig. 8b). Models of the effects of varying overlap (not shown) indicate that slip along the step-bounding fault segments

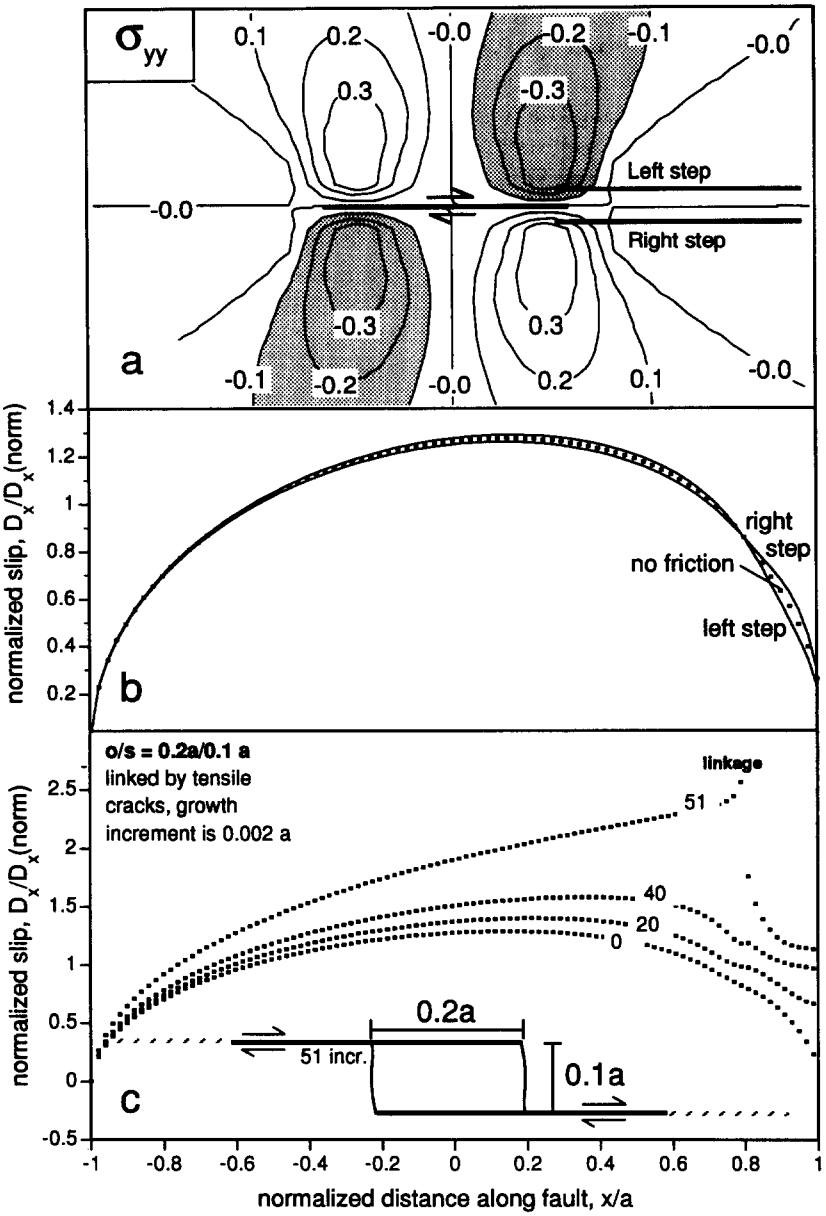

Fig. 9. (a) Contoured distribution of the fault-normal stress, σ_{yy}, about a slipped fault. (b) Slip distribution along frictional right-lateral echelon fault segments with $0.1a$ overlap and $0.1a$ separation. Because the stress boundary conditions along the faults depend on the normal stress, σ_{yy}, the slip distributions of left- and right-stepping echelon faults differ. (c) Influence of opening fractures in a right step (at splay-fracture lengths of 0, 20, 40 and 51 times $0.002a$) on fault slip distributions. Inset shows the paths of the fractures emanating from the fault terminations according to a maximum circumferential stress criterion. Remote and crack stress boundary conditions are same as in Fig. 8(a).

is reduced due to a stress shadowing effect if overlap is large. However, if faults overlap by only a small fraction of their length, or if they underlap, slip is increased at small separations.

In the previous discussion we neglected the effects of non-uniform fault-normal stresses due to mechanical interaction. Figure 9(a) shows the contoured magnitude of the fault-normal stress, σ_{yy}, about a single right-lateral fault with the same boundary conditions as in the previous model. In a right-stepping arrangement the adjacent fault will be exposed to fault-normal tensile stress near the overlapping region. If faulting is frictional, the reduced fault-normal compressive stress will reduce frictional stress and increase slip (Segall & Pollard 1980, Aydin & Schultz 1990). The opposite is to be expected for the left-stepping geometry where the end zones of the overlapping faults reside in a zone of increased fault-normal compression (shaded zones in Fig. 9a).

We apply a Coulomb failure condition to the faults, $\sigma^c_{yx} = \mu\,\sigma_{yy}$, with a coefficient of friction μ of 0.6. Where fault-normal compressive stress is increased, slip will be reduced. With a step geometry of $0.1a$ overlap and $0.1a$ separation we find that friction causes a reduction of slip along the step bounding fault segments about left steps and an increase of slip about right steps (Fig. 9b). However, the slip distributions are not greatly different from the frictionless case. These different situations probably would be difficult to distinguish using slip data from real faults.

Where two strike-slip fault segments are arranged in an echelon geometry, stress perturbations may favor the development of inelastic deformation around the

stepover (Segall & Pollard 1980, Sibson 1986, Gamond 1987, Aydin & Schultz 1990, Bürgmann & Pollard 1993). We investigate the effects of inelastic deformation at fault steps by allowing opening fractures to grow from the echelon fault ends of a right step between two right-lateral fault segments (Fig. 9c). If the opening cracks propagate across the step, they effectively link the segments, and transfer slip. We find that the slip distribution along the faults approaches that of a single fault of the combined length of the two segments as the open fractures approach linkage. Similarly, mass solution transfer out of contractional fault steps through the development of pressure solution seams (Gamond 1987) or pressure-enhanced ductile strain accommodation in steps allows the effective transfer of displacement between echelon faults (Bürgmann & Pollard 1994).

Figure 5(a) shows an example of strongly asymmetric slip distributions along echelon faults near Kirkcudbright, Scotland that were mapped by Peacock (1991) in comparison with results from an elastic model of two right-stepping, left-lateral echelon faults with strong end zones and inelastic deformation in the stepover region. To account for ductile flow in a shale layer that encloses the fault stepover (Fig. 5a, inset) we include a fault-perpendicular anticrack (Fletcher & Pollard 1981) between the two model faults. Interpenetration of the anticrack walls represents inelastic strain accommodation in the step. Furthermore, we introduce two strong end zones at the distal fault terminations where $\sigma^{h}_{yx} = 1.5\,\sigma^{r}_{yx}$, to model the effects of lateral fault growth that may have caused the tapered slip distribution. The model (Fig. 5a, filled circles) correctly predicts the relative slip magnitudes, however, the mechanisms used here are not unique. Independent evidence for their application to these data is needed to make this a convincing explanation.

Effects of changes in elastic moduli on slip distributions

We now address how heterogeneity in one elastic parameter, the Young's modulus of the rock, can affect slip along a fault. We focus on the influence of a single inclusion of different moduli on a single fault in an otherwise homogeneous and infinite body. The inclusion could represent, for example, an igneous body or a sedimentary unit that is more or less stiff than the surrounding rock. The model fault lies along the x-axis and has a unit half-length, whereas the inclusions are rectangular, of finite size, and have edges parallel to the x- and y-axes (Fig. 10a, inset).

We examine three different geometries (see insets in Fig. 10): (1) the fault is completely outside but terminates at the boundary of the inclusion; (2) the fault cuts across the inclusion and terminates in the surrounding rock; and (3) the fault cuts to the center of the inclusion. For each geometry we present results of trials where, E^*/E, the ratio of the Young's modulus in the inclusion to that in the host material, was set to 0.1, 0.5, 1, 2, and 10. Poisson's ratio is 0 for both the inclusion and the host.

The fault is divided into a series of 40 contiguous elements of equal length. The fault sustains no shear stress and is subject to a uniform remote unit shear stress $\sigma^{r}_{yx} = 1$ MPa, whereas σ^{r}_{xx} and σ^{r}_{yy} are zero. With these boundary conditions and geometries, the fault walls do not interpenetrate or open. Two coincident contours define the interface between the inclusion and the host material. One contour bounds the exterior of the inclusion, whereas the second marks an interior boundary of the host material. Each contour is divided into a series of boundary elements. The solution technique requires that displacements as well as normal and shear tractions be continuous across the two interface contours. To ensure that smooth slip distributions are obtained along the fault, the interface boundary elements in the vicinity of the fault are slightly shorter than the elements on the fault itself.

The normalized slip is plotted vs the normalized position along the fault in Fig. 10. The case, $E^*/E = 1$, a homogeneous body, serves as a reference. Five effects of material heterogeneity stand out clearly in these figures, the first being especially central to the main theme of this paper:

(1) The slip distribution can be significantly distorted from a symmetric elliptical profile if Young's modulus varies near the fault by more than a factor of two. The distortion increases as the disparity between the modulus of the host and the inclusion increases. Depending on the location of the inclusion, the profile can be smooth and tear-drop shaped (Fig. 10a), symmetrical but non-elliptical (Fig. 10b), or asymmetric and irregular (Fig. 10c). For inclusions with a low modulus near the termination of a fault, the maximum slip is shifted towards the inclusion (Fig. 10a). Note that a non-symmetric and non-elliptical slip distribution may result even if an inclusion were merely near a fault; material heterogeneities need not be visible along a fault to affect the slip distribution.

(2) The amount of slip increases everywhere along a fault if the inclusion is softer (lower Young's modulus) than the host, but decreases if the inclusion is stiffer than the host. Changes in slip from the reference (homogeneous) case are most pronounced near the inclusion and decrease with distance from it. Accordingly, the effects are most pronounced if and where part of the fault is in contact with an inclusion. Soft inclusions cut by faults induce larger effects than stiff ones. For example, in Fig. 10(b), a 10-fold decrease of inclusion modulus relative to the host results in a maximum slip value of about 3.5 times that of the reference case, whereas a 10-fold increase of inclusion modulus leads to a decrease in maximum slip to only 0.6 times the reference case.

(3) For very stiff inclusions the slip profile will be nearly flat along the part of the fault in contact with the inclusion. A very stiff inclusion essentially will be displaced as a rigid body and will deform relatively little internally.

(4) Sharp gradients in slip can develop along a fault near the interface between the host and the inclusion, with the gradient increasing as the difference in modulus

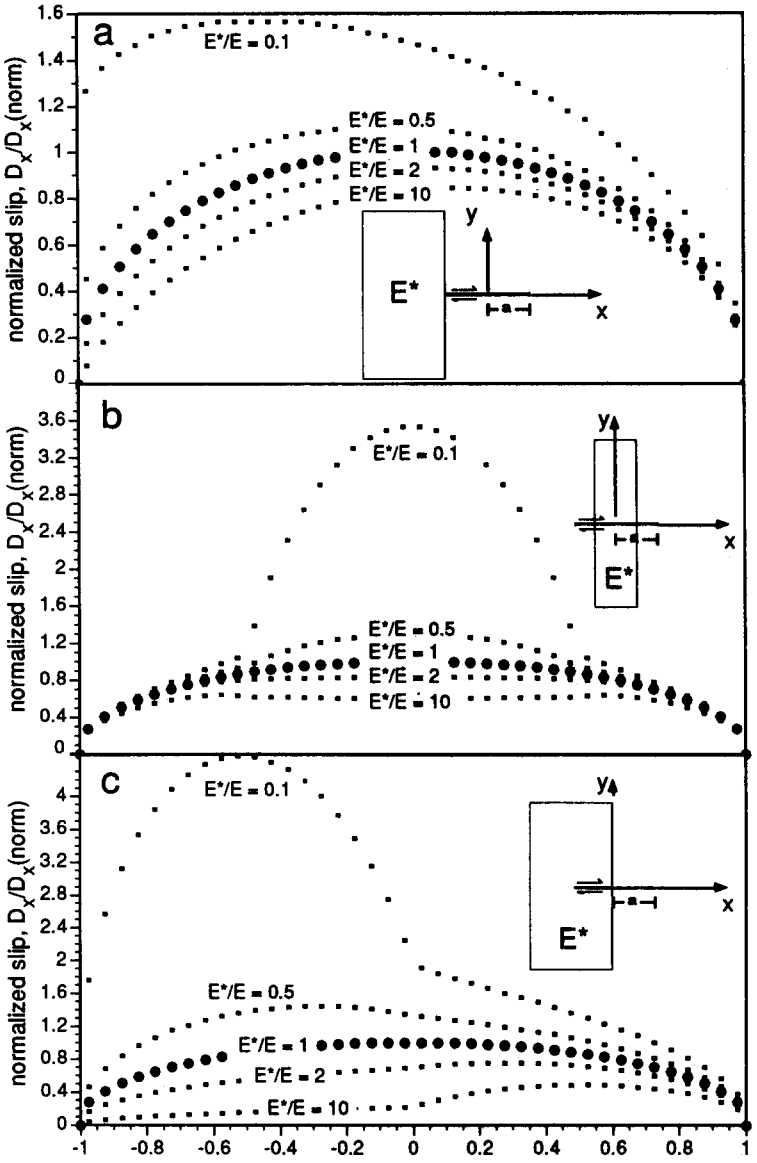

Fig. 10. (a) Slip distributions for a fault that abuts an inclusion of different modulus (see inset). Ratios of Young's modulus in the inclusion to that in the host (E^*/E) range from 0.1 to 10. (b) Slip distributions for a fault that cuts an inclusion (see inset). Ratios of Young's modulus in the inclusion to that in the host (E^*/E) range from 0.1 to 10. (c) Slip distributions for a fault that is partly enclosed within a rectangular inclusion (see inset). Ratios of Young's modulus in the inclusion to that in the host (E^*/E) range from 0.1 to 10.

increases. In contrast, for faults subject to uniform driving stresses in homogeneous materials, sharp gradients in slip would occur only near the fault ends (Fig. 4a). If moduli along a fault were sufficiently different, the attendant slip gradients could become steep enough that dilatant splay fractures form near the interface; such fractures typically are restricted to near the ends of isolated faults in relatively homogeneous materials (Segall & Pollard 1983, Martel *et al.* 1988).

(5) The slip profiles for the heterogeneous bodies studied here are convex everywhere except in the immediate vicinity of a material interface (Fig. 10). In contrast, for non-uniform driving stress the profiles may be convex along some portions of the fault but concave elsewhere (Figs. 4b and 6). The sense of curvature along a slip profile perhaps could offer a way to distinguish causes for non-elliptic slip distributions.

Muraoka and Kamata (1983) speculated that changes in competence of the host rock may influence the slip distribution of faults breaking through various sedimentary rock types. The less competent (in its current state) sandstone in Fig. 5(b) is thought to reduce fault slip by ductile drag (Muraoka & Kamata 1983). Alternatively, a reduction of slip would be expected if the sandstone were stiffer. Our modeling (Fig. 5b, triangles) shows that the slip distribution could be roughly approximated if the Young's modulus of the sandstone were about five times greater than that of the siltstone. Such a ratio is not unreasonable given the elastic values for sandstone and shale in the technical literature (e.g. Hatheway & Kiersch 1990).

Another possible explanation is that the sandstone had a greater frictional resistance to slip. We can model these conditions by applying a slip retarding shear stress boundary condition on the fault segment in the sandstone. The modeled slip distribution (Fig. 5b, squares)

closely matches the observed slip (Fig. 5b, open circles). Based on the sense of curvature of the profile in the sandstone, the slip profile of Muraoka & Kamata (1983) is fit better by a model with heterogeneous strength on the fault than by a model with heterogeneous materials and a constant stress drop. However, without further testing of the constitutive and frictional properties of the host rock we are not able to definitively discriminate between the different explanations.

DISCUSSION AND CONCLUSIONS

We have identified and quantified several factors that influence the slip distributions along faults. Our model results show that deviations from an idealized symmetrical and elliptical slip distribution are caused by stress gradients, heterogeneous elastic properties, inelastic deformation processes, and mechanical interaction between adjacent fault segments. Some of these factors can be recognized in previously published examples of slip distributions (e.g. Muraoka & Kamata 1983, Walsh & Watterson 1990, Peacock 1991, Scholz *et al.* 1993).

As faults propagate through previously intact rock, the resistance to slip near the fault periphery may be greater than that near the mature center. Similarly, if the friction changes with slip magnitude along a fault, this non-uniform resistance influences the slip distribution. Tapered slip distributions toward fault tips have been cited as evidence for inelastic deformation during fault growth (Cowie & Scholz 1992b, Scholz *et al.* 1993), but such distributions can be produced in purely elastic models with non-uniform loading. Tapered slip distributions also have been cited as evidence for fault propagation with a plastic yield zone and finite tip stresses (the so-called Dugdale–Barenblatt model). However, this model requires that the derivative of slip with respect to position along the fault goes to zero at the tip. Published field data do not define slip distributions well enough near fault tips to make conclusive statements about these models (e.g. Dawers *et al.* 1993, Scholz *et al.* 1993).

If stress concentrations near fault terminations induced permanent deformation in the host rock, the development of secondary structures (fractures, folds and fabric) will cause further deviations from slip distributions derived from simple models. Some faults are part of a larger fault zone and are expected to strongly influence slip distributions of their nearest neighbors because of perturbations of the local stress field. Single fault segments may be effectively linked by secondary structures in the stepover region. Faults in heterogeneous host rocks such as normal faults in stratified rocks will show localized slip maxima in softer units. Even if the fault does not cut through a nearby body of different elastic modulus, its slip distribution will be affected. Clearly it is important to analyze slip distributions in the context of a fault's three-dimensional geometry, its relationship to nearby structures, the constitutive behavior of the host rock, and the development of secondary structures. Documentation of this context requires detailed mapping of the fault(s) and the surrounding rock.

Recently, attention has focused on scaling laws relating slip magnitude to the dimension of a fault and related fault growth models (e.g. Walsh & Watterson 1988, Cowie & Scholz 1992a, Scholz *et al.* 1993). Fault slip distributions from a variety of tectonic and geologic settings commonly are represented by points on log–log plots of maximum slip vs fault trace length. Such representations may be useful from some standpoints, but they fail to shed light on (and tend to divert attention from) a host of key issues relevant to understanding and predicting the slip behavior of faults. Our results suggest that more detailed field descriptions, maps, and analyses of more realistic slip distributions are needed to address the scaling laws for faulting.

Acknowledgements—This research was supported by the Rock Fracture Project of Stanford University and NSF grant EAR-9017909. John Walsh, Chris Scholz and Associate Editor Jim Evans provided very helpful reviews. David Pollard would like to thank David Peacock and Patience Cowie for interesting discussions that helped focus his attention on these problems. Also, he would like to thank the organizers of the 17th Fungal Genetics Conference (Asilomar, CA, March 1993) for providing an appropriate place to study the Westergaard stress functions.

REFERENCES

Antonellini, M. A., Aydin, A. & Pollard, D. 1994. Microstructure of deformation bands in porous sandstones at Arches National Park, Utah. *J. Struct. Geol.* **16** (7), 941–959.

Archuleta, R. 1984. A faulting model for the 1979 Imperial Valley earthquake. *J. geophys. Res.* **89**, 4559–4585.

Atkinson, B. K. & Meredith, P. G. 1987. Experimental fracture mechanics data for rocks and minerals. In: *Fracture Mechanics of Rock* (edited by Atkinson, B. K.). Academic Press Inc. London, 477–525.

Aydin, A. 1978. Small faults formed as deformation bands in sandstone. *Pure & Appl. Geophys.* **116**, 913–930.

Aydin, A. & Schultz, R. A. 1990. Effect of mechanical interaction on the development of strike-slip faults with echelon patterns. *J. Struct. Geol.* **12**, 123–129.

Barenblatt, G. I. 1962. The mathematical theory of equilibrium cracks in brittle fracture. *Adv. Appl. Mech.* **7**, 55–125.

Barnett, J. A. M., Mortimer, J., Rippon, J. H., Walsh, J. J. & Watterson, J. 1987. Displacement geometry in the volume containing a single normal fault. *Bull. Am. Ass. Petrol. Geol.* **71**, 925–937.

Barquins, M. & Petit, J. P. 1992. Kinetic instabilities during the propagation of a branch crack: effects of the loading conditions and internal pressure. *J. Struct. Geol.* **14**, 893–903.

Beroza, G. C. 1991. Near-source modeling of the Loma Prieta earthquake: evidence for heterogeneous slip and implications for earthquake hazard. *Bull. seism. Soc. Am.* **81**, 1603–1621.

Bilham, R. & Bodin, P. 1992. Fault zone connectivity: Slip rates on faults in the San Francisco Bay area, California. *Science* **258**, 281–284.

Bilham, R. & King, G. C. P. 1989a. The morphology of strike-slip faults: examples from the San Andreas fault, California. *J. geophys. Res.* **94**, 10204–10216.

Bilham, R. & King, G. C. P. 1989b. Slip distribution on oblique segments of the San Andreas fault, California: Observations and theory. *Open File Rep. U.S. geol. Surv.* **89-315**, 80–93.

Bouvier, J. D., Kaars-Sijpesteijn, C. H., Kluesner, D. F., Onyejekwe, C. C. & van der Pal, R. C. 1989. Three-dimensional seismic interpretation and fault sealing investigations, Nun River Field, Nigeria. *Bull. Am. Ass. Petrol. Geol.* **73**, 1397–1414.

Bürgmann, R. & Pollard, D. D. 1992. Influence of the state of stress on the brittle–ductile transition in granitic rock: evidence from fault steps in the Sierra Nevada, California. *Geology* **20**, 645–648.

Bürgmann, R. & Pollard, D. D. 1994. Strain accommodation about strike-slip fault discontinuities in granite rock under brittle-to-ductile conditions. *J. Struct. Geol.* **12**, 1655–1674.

Chapman, T. J. & Meneilly, A. W. 1991. The displacement patterns associated with a reverse-reactivated, normal growth fault. In: *The Geometry of Normal Faults* (edited by Roberts, A. M., Yielding, G. & Freeman, B.). *Spec. Publ. geol. Soc. Lond.* **56**, 183–191.

Christie-Blick, N. & Biddle, K. T. 1985. Deformation and basin formation along strike-slip faults. In: *Strike-slip Deformation, Basin Formation, and Sedimentation, Spec. Publ.*, 37 (edited by Biddle, K. T. & Christie-Blick, N.). Society of Economic Paleontologists and Mineralogists, Tulsa, Okla, 1–34.

Cowie, P. A. & Scholz, C. H. 1992a. Growth of faults by accumulation of seismic slip. *J. geophys. Res.* **97**, 11085–11095.

Cowie, P. A. & Scholz, C. H. 1992b. Physical explanation for the displacement–length relationship of faults using a post-yield fracture mechanics model. *J. Struct. Geol.* **14**, 1133–1148.

Crouch, S. L. & Starfield, A. M. 1983. *Boundary Element Methods in Solid Mechanics*. Unwin Hyman, London.

Crowell, J. C. 1974. Sedimentation along the San Andreas fault, California. In: *Modern and Ancient Geosynclinal Sedimentation* (edited by Dott, R. H. & Shaver, R. H.). *Spec. Publs Soc. econ. Paleont. Miner.* **19**, 292–303.

Dawers, N. H., Anders, M. H. & Sholz, C. H. 1993. Growth of normal faults: Displacement–length scaling. *Geology* **21**, 1107–1110.

Delaney, P. T. & Pollard, D. D. 1981. Deformation of host rocks and flow of magma during growth of minette dikes and breccia-bearing intrusions near Ship Rock, New Mexico. *Prof. Pap. U. S. geol. Surv.* **1202**.

Deng, Q., Wu, D., Zhang, P. & Chen, S. 1986. Structure and deformational character of strike-slip fault zones. *Pure & Appl. Geophys.* **124**, 203–224.

Dugdale, D. S. 1960. Yielding of steel sheets containing slits. *J. Mech. Phys. Solids* **8**, 100–104.

Erdogan, F. & Sih, G. C. 1963. On the crack extension in plates under plane loading and transverse shear. *J. Basic Engin.* 519–527.

Eshelby, J. D. 1957. The determinations of the elastic field of an ellipsoidal inclusion and related problems. *Proc. R. Soc. Lond.* **A241**, 376–396.

Fletcher, R. & Pollard, D. D. 1981. An anticrack mechanism for stylolites. *Geology* **9**, 419–424.

Gamond, J. F. 1987. Bridge structures as sense of displacement criteria in brittle fault zones. *J. Struct. Geol.* **9**, 609–620.

Gillespie, P. A., Walsh, J. J. & Watterson, J. 1992. Limitations of dimension and displacement data from single faults and the consequences for data analysis and interpretation. *J. Struct. Geol.* **14**, 1157–1172.

Granier, T. 1985. Origin, damping and pattern of development of faults in granite. *Tectonics* **4**, 721–737.

Harris, R. & Segall, P. 1987. Detection of a locked zone at depth on the Parkfield, California segment of the San Andreas fault. *J. geophys. Res.* **92**, 7945–7962.

Hatheway, A. W. & Kiersch, G. A. 1990. Engineering properties of rock. In: *Physical Properties of Rocks and Minerals* (edited by Carmichael, R. S.). CRC Press Boca Raton, Florida, 671–715.

Higgs, W. G. & Williams, G. D. 1987. Displacement efficiency of faults and fractures. *J. Struct. Geol.* **9**, 371–374.

Ida, Y. 1972. Cohesive force across the tip of a longitudinal-shear crack and Griffith's specific surface energy. *J. geophys. Res.* **77**, 3796–3805.

Kanninen, M. F. & Popelar, C. H. 1985. *Advanced Fracture Mechanics*. Oxford University Press, New York.

Lawn, B. R. & Wilshaw, T. R. 1975. *Fracture of Brittle Solids*. Cambridge University Press, Cambridge.

Lawson, J. J. 1908. The California earthquake of 18 April 1906: Report of the State Earthquake Investigation Commission. *Carnegie Institution of Washington Publication* **87**.

Li, V. C. 1987. Mechanics of shear rupture applied to earthquake zones. In: *Fracture Mechanics of Rock* (edited by Atkinson, B. K.). Academic Press Inc. London, 351–428.

Martel, S. J. & Pollard, D. D. 1989. Mechanics of slip and fracture along small faults and simple strike-slip fault zones in granitic rock. *J. geophys. Res.* **94**, 9417–9428.

Martel, S. J., Pollard, D. D. & Segall, P. 1988. Development of simple strike-slip fault zones in granitic rock, Mount Abbot quadrangle, Sierra Nevada, California. *Bull. geol. Soc. Am.* **99**, 1451–1465.

Muraoka, H. & Kamata, H. 1983. Displacement distribution along minor fault traces. *J. Struct. Geol.* **5**, 483–495.

Muskhelishvili, N. E. 1954. *Some Basic Problems of the Mathematical Theory of Elasticity*. P. Noordhof, Leyden, Netherlands.

Nemat-Nasser, S. & Horii, H. 1982. Compression-induced nonplanar crack extension with application to splitting, exfoliation, and rockburst. *J. geophys. Res.* **87**, 6805–6821.

Palmer, A. C. & Rice, J. R. 1973. The growth of slip surfaces in the progressive failure of overconsolidated clay. *Proc. R. Soc. Lond.* **A332**, 527–548.

Peacock, D. C. P. 1991. Displacements and segment linkage in strike-slip fault zones. *J. Struct. Geol.* **13**, 1025–1035.

Petit, J. P. 1987. Criteria for the sense of movement on fault surfaces in brittle rock. *J. Struct. Geol.* **9**, 597–608.

Petit, J. P. & Barquins, M. 1988. Can natural faults propagate under mode II conditions? *Tectonics* **7**, 1243–1256.

Pollard, D. D. & Muller, O. H. 1976. The effect of gradients in regional stress and magma pressure on the form of sheet intrusions in cross-section. *J. geophys. Res.* **81**, 975–984.

Pollard, D. D. & Segall, P. 1987. Theoretical displacements and stresses near fractures in rocks: With applications to faults, joints, veins, dikes, and solution surfaces. In: *Fracture Mechanics of Rock* (edited by Atkinson, B. K.). Academic Press Inc., London, 277–349.

Reasenberg, P. A. & Simpson, R. W. 1992. Response of regional seismicity to the static stress change produced by the Loma Prieta earthquake. *Science* **255**, 1687–1690.

Rippon, J. H. 1985. Contoured patterns of the throw and hade of normal faults in the Coal Measures (Westphalian) of north-east Derbyshire. *Proc. Yorks. geol. Soc.* **45**, 147–161.

Rodgers, D. A. 1980. Analysis of pull-apart basin development produced by en échelon strike-slip faults. In: *Sedimentation in Oblique-slip Mobile Zones* (edited by Ballance, P. F. & Reading, H. G.). *Spec. Publ. Int. Assoc. Sedimentol.* **4**, 27–41.

Rudnicki, J. W. 1980. Fracture mechanics applied to the Earth's crust. *Ann. Rev. Earth & Planet. Sci.* **8**, 489–525.

Rymer, M. J. 1989. Surface rupture in a fault stepover on the Superstition Hills fault, California. In: *Fault Segmentation and Controls of Rupture Initiation and Termination* (edited by Schwartz, D. P. & Sibson, R. H.). *U.S. Geol. Surv. Open-File Report* **89–315**, 309–323.

Scholz, C. H., Dawers, N. H., Yu, J. Z. & Anders, M. H. 1993. Fault growth and fault scaling laws: Preliminary results. *J. geophys. Res.* **98**, 21,951–21,961.

Segall, P. & Pollard, D. D. 1980. Mechanics of discontinuous faults. *J. geophys. Res.* **85**, 4337–4350.

Segall, P. & Pollard, D. D. 1983. Nucleation and growth of strike-slip faults in granite. *J. geophys. Res.* **88**, 555–568.

Sibson, R. H. 1986. Rupture interaction with fault jogs. In: *Earthquake Source Mechanics, AGU Geophysical Monograph* (edited by Das, S., Boatwright, J. & Scholz, C.). American Geophysical Union **37**, Washington, D. C., 157–168.

Sieh, K. 1978. Slip along the San Andreas fault associated with the great 1857 earthquake. *Bull. seism. Soc. Am.* **68**, 1421–1428.

Tada, H., Paris, P. C. & Irwin, G. R. 1973. *The Stress Analysis of Cracks Handbook*. Del Research Corporation, Hellertown, Pennsylvania.

Thatcher, W. & Lisowski, M. 1987. Long-term seismic potential of the San Andreas fault southeast of San Francisco, California. *J. geophys. Res.* **92**, 4771–4784.

Thomas, A. L. & Pollard, D. D. 1993. The geometry of echelon fractures in rock: Implications from laboratory and numerical experiments. *J. Struct. Geol.* **15**, 323–334.

Tschalenko, J. S. 1970. Similarities between shear zones of different magnitudes. *Bull. geol. Soc. Am.* **81**, 1625–1640.

Vedder, J. G. & Wallace, R. E. 1970. Map showing recently active breaks along the San Andreas and related faults between Cholame Valley and Tejon Pass, California. *U.S. Geol. Surv. Misc. Field Investig. Map* **I-574**.

Wald, D. J., Helmberger, D. V. & Hartzell, S. H. 1990. Rupture process of the 1987 Superstition Hills earthquake from the inversion of strong-motion data. *Bull. seism. Soc. Am.* **80**, 1079–1098.

Wallace, R. E. 1973. Surface fracture patterns along the San Andreas Fault. In: *Conference on Tectonic Problems of the San Andreas Fault System, Proceedings* (edited by Kovach, R. L. & Nur, A.). Stanford University Publications, *Geol. Sci.* **13**, 248–250.

Walsh, J. J. & Watterson, J. 1987. Distribution of cumulative displacement and of seismic slip on a single normal fault surface. *J. Struct. Geol.* **9**, 1039–1046.

Walsh, J. J. & Watterson, J. 1988. Analysis of the relationship between displacements and dimensions of faults. *J. Struct. Geol.* **10**, 239–247.

Walsh, J. J. & Watterson, J. 1989. Displacement gradients on fault surfaces. *J. Struct. Geol.* **11**, 307–316.

Walsh, J. J. & Watterson, J. 1990. New methods of fault projection for coalmine planning. *Proc. Yorks. geol. Soc.* **48**, 209–219.

Walsh, J. J. & Watterson, J. 1991. Geometric and kinematic coherence and scale effects in normal fault systems. In: *The Geometry of Normal Faults* (edited by Roberts, A. M., Yielding, G. & Freeman, B.). *Spec. Publs geol. Soc. Lond.* **56**, 193–203.

Watterson, J. 1986. Fault dimensions, displacements and growth. *Pure & Appl. Geophys.* **124**, 365–373.

Westergaard, H. M. 1939. Bearing pressures and cracks. *J. Appl. Mech.* **66**, A49–A53.

Zoback, M. D. & Zoback, M. L. 1991. Tectonic stress field of North America and relative plate motions. In: *Neotectonics of North America, The Decade of North American Geology Project Series* (edited by Slemmons, D. B., Engdahl, E. R., Zoback, M. D. & Blackwell, D. D.). Geol. Soc. Am. Boulder, Colorado, 339–366.